RESEARCH ARTICLE

Lamellar Degradation Induced Brittle-ductile Transition of Polysynthetic Twinned TiAl

Henggao Xiang[1,2,†], **Demin Zhu**[1,†], **Xu Liu**[1], **Yang Chen**[1,2,*], **Zhixiang Qi**[1,2,*] **and Guang Chen**[1]

[1] State Key Laboratory of Light Superalloys / Advanced Casting Technologies, Nanjing University of Science and Technology, Nanjing 210094, China
[2] Jiangsu Belight Laboratory, Nanjing University of Science and Technology, Nanjing 210094, China

Abstract

Intermetallic compounds including TiAl and NiAl suffer from an abrupt brittle-ductile transition at a critical temperature, limiting their higher temperature applications. Conventional viewpoints attribute this transition to thermally activated dislocation actions or dynamic recrystallization. Here, we discover a novel brittle-ductile transition mechanism in polysynthetic twinned TiAl, driven by lamellar degradation, which significantly deviates from the conventional mechanisms. The results demonstrate that the lamellar degradation is primarily caused by the $\alpha_2 \rightarrow \gamma$ phase transformation at the brittle-ductile transition temperature, which stems from a non-monotonic increase in the stacking fault energy of α_2 phase with temperature. This unconventional transition can be described efficiently by an energy density-based strength model, offering new insights into the brittle-ductile transition behavior of intermetallic compounds at elevated temperatures.

Keywords: polysynthetic twinned TiAl, brittle-ductile transition, lamellar degradation, high temperature strength.

1 Introduction

The brittle-ductile transition (BDT) is a common phenomenon in intermetallic compounds [1, 2]. Deformation behavior undergoes a fundamental change from brittle to ductile fracture below a critical temperature, termed the brittle-ductile transition temperature (BDTT) [3, 4]. While the enhancement in ductility above the BDTT confers improved ductility, it concurrently leads to a marked reduction in strength, restricting the higher temperature application of these intermetallic compounds [5, 6]. Consequently, a comprehensive insight into the mechanism governing the BDT in intermetallic compounds is critical for their wider applications [7, 8].

As a typical intermetallic compound, TiAl alloys have been successfully employed in replacing Ni-based superalloys in low pressure turbine blades [9, 10] due to their high strength and creep resistance, with the advantage of a mass decrease of up to 50%

Submitted: 20 November 2025
Accepted: 17 December 2025
Published: 29 December 2025

Vol. 1, **No.** 1, 2025.
10.62762/JAMR.2025.522742

***Corresponding authors:**
✉ Yang Chen
yang.chen@njust.edu.cn
✉ Zhixiang Qi
zxqi@njust.edu.cn

† These authors contributed equally to this work

Citation
Xiang, H., Zhu, D., Liu, X., Chen, Y., Qi, Z., &Chen, G. (2025). Lamellar Degradation Induced Brittle-ductile Transition of Polysynthetic Twinned TiAl. *Journal of Advanced Materials Research*, 1(1), 56–68.

© 2025 by the Authors. Published by Institute of Central Computation and Knowledge. This is an open access article under the CC BY license (https://creativecommons.org/licenses/by/4.0/).

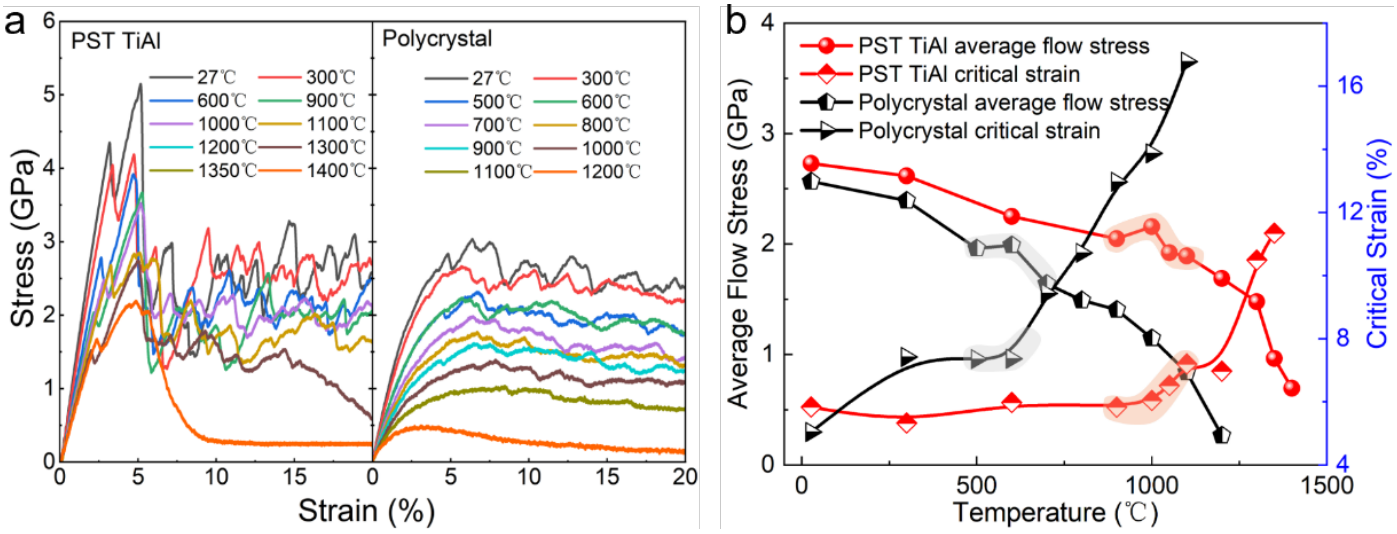


Figure 1. Stress-strain relations and flow stress from MD simulations of PST TiAl and polycrystal TiAl. a) Simulated stress-strain curves at different temperatures; b) Average flow stress and critical strain vary with temperatures.

[11–14]. However, polycrystal TiAl alloys undergo a BDT between 650 and 750 °C, driven primarily by dislocations or dynamic recrystallization [15, 16], limiting their application at higher temperatures. By eliminating grain boundaries, polysynthetic twinned (PST) TiAl achieve a significant increase in high-temperature strength and 1–2 orders of magnitude improvement in creep life. Consequently, PST TiAl extend their service temperature to over 900 °C [11, 12, 17]. However, an in-depth understanding of the BDT mechanism in PST TiAl remains elusive.

In this study, we conduct molecular dynamics (MD) simulations and experiments to investigate the BDT behaviors of PST TiAl. The results elucidate lamellar degradation induced BDT, which deviates from the conventional dislocation actions or dynamic recrystallization. We then propose an energy density-based strength model to describe the unconventional transition, providing a theoretical foundation for enhancing the high-temperature performance of TiAl alloys.

2 Results and Discussion

2.1 Brittle-ductile transition mechanism of PST TiAl

To obtain the entire process of BDT mechanism, we first conducted molecular dynamics (MD) simulations. The stress-strain curves of PST TiAl and polycrystal TiAl obtained by MD simulations at different temperatures are presented in Figure 1. It is shown that the curves of both PST TiAl and polycrystal TiAl exhibit a linear relationship in the elastic stage, and the elastic modulus decreases with rising temperature due to the bond weakening at high-temperature [18, 19]. In the plastic stage, as shown in Figure 1(b), the average flow stress decreases with increasing temperature and critical strain increases in both alloys before the BDTT, in qualitative agreement with experimental observations [20, 21]. It is interesting to see that the BDTT of PST TiAl occurs above 1000 °C, much higher than the 600 °C of polycrystal. In experiments, the BDTT for high-niobium TiAl polycrystals was observed to be 760–780 °C [22], while that for single crystals was above 900 °C [11], which is close to the results obtained from our simulation. Following the BDTT, both alloys exhibit a sharp drop in flow stress accompanied by a significant increase in critical strain, which is typical characteristic of BDT behavior [23]. In addition, both alloys exhibit anomalous yield before BDTT, which has been widely observed in intermetallic compounds [24, 25].

To elucidate the underlying mechanism of BDT in PST TiAl, we simultaneously conducted deformation analysis via simulations and experiments near BDTT. As shown in Figure 2, the deformations exhibit significant temperature-dependent characteristics. At 900 °C, high-density stacking faults are predominantly observed in γ phase following plastic deformation, whereas the α_2 phase exhibits minimal deformation microstructure (Figure 2(a)). This suggests that the γ phase is more susceptible to deformation under this temperature, due to its lower resistance to slip than the α_2 phase. Figure 2(b) confirms that stacking faults in the γ lamellae dominate the deformation behavior at 900 °C through transmission electron microscopy (TEM). Uniform stacking faults appear in the γ phase,

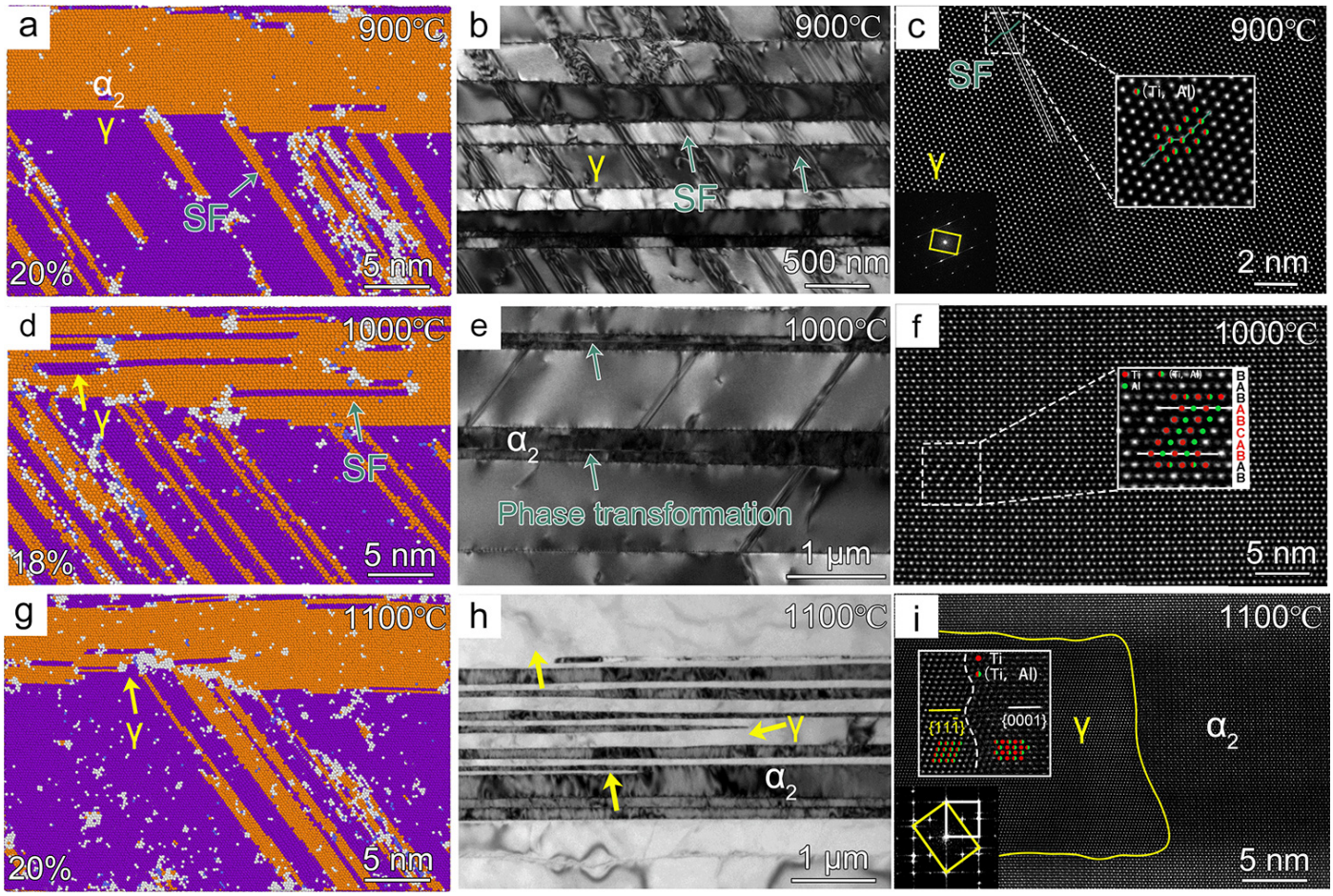


Figure 2. Microstructural characteristics after deformation of PST TiAl through MD simulation, TEM characterization and HAADF-STEM images at 900 °C (a–c), 1000 °C (d–f) and 1100 °C (g–i).

resulting in a uniform distribution of overall strain and coordinated deformation to avoid premature failure. And the original structure remains in α_2, allowing the material to maintain high temperature strength. Figure 2(c) provides a magnified view of a stacking fault composed of only two atomic layers, as observed through HAADF-STEM along the $< 011]$ zone axis. This atomic misalignment can hinder the movement of dislocations, allowing the material to maintain or even increase its high-temperature strength [26, 27].

The deformation mechanism at 1000 °C is markedly different from other temperatures, as shown in Figure 2(d). The stacking faults further increase and become more uniformly distributed within the γ lamellae. Notably, stacking faults and phase transformation are observed in α_2 phase (green arrows). The formation of stacking faults in α_2 phase is governed by the activation barrier of crystallographic slip systems and the stability of chemical bonds [28, 29]. At elevated temperatures, reduced stacking fault energy induces the creation of phase transformation through stacking faults accumulation [30, 31]. In the HAADF images (Figure 2(f)), five-layer atoms of the γ phase were observed in the α_2 phase, demonstrating the initiation of phase transformation under stress at this temperature. The stacking faults in α_2 phase can serve as nano-scale nucleation sites for the γ phase. Meanwhile, the high-density stacking faults in the γ phase lead to a significant abnormal yield effect, while the dislocation and phase transformation-induced coordinated deformation in α_2 make the material less prone to premature failure.

The α_2/γ flat interface is disrupted and γ phase grows towards α_2 phase at 1100 °C, as shown in Figure 2(g). The periodicity of the $D0_{19}$ structure has been disrupted in the vicinity of the α_2/γ interface, facilitating atomic reorganization into the close-packed planes of the γ phase ($L1_0$ structure) through stacking faults induced interface migration, without requiring long-range diffusion. The interface migration is driven by the non-monotonic temperature dependence of the stacking fault energy (SFE) of α_2 phase. Specifically, the SFE exhibits an initial decrease with temperature, reaching a minimum at 1100 °C,

followed by a subsequent increase (Figure A1(a)). Meanwhile, disordered clusters appear in the γ and α_2 phases at 1100 °C, which are precursors of stacking fault deformation and promote the formation of stacking faults. Simultaneously, when the interface migration occurs, the stacking fault density within the γ phase significantly decreases. The yellow arrow in Figure 2(g) exhibits pile-up of stacking faults at phase interfaces, the accumulation of these defects during deformation may trigger interface migration and degradation of α_2 lamellae. The lamellar degradation reduces overall structural stability, thereby leading to a decrease in the flow stress. The TEM image in Figure 2(h) also reveals the features of lamellar degradation observed during the simulation. The degradation occurs not only at the interface but also manifests transformation features within the α_2 phase itself due to thermal activation [32].

The HADDF image in Figure 2(i) reveals an indistinct interface between the α_2 and γ phases, indicating that lamellar degeneration is caused by the $\alpha_2 \rightarrow \gamma$ phase transformation. Thus, it can be concluded that the abnormal yielding at 1000 °C is attributed to the uniformly distributed high-density stacking faults, while the accelerated decline in yield strength over 1000 °C primarily stems from the degradation of α_2 lamellae. Additionally, the strain concentration at 1100 °C is higher than that at 900 and 1000 °C (Figure A2), indicating that lamellar degradation over 1000 °C is more likely to lead to BDT. In comparison, the significant local strain concentration caused by grain boundaries in polycrystals leads to BDT at 600 °C (Figure A3).

At 1200 °C, there is no significant change in the stacking fault density, while the number of disordered atoms increases, as shown in Figure 3(a). It is worth noting that within the temperature range of 1100 to 1200 °C, although minor disordered atomic aggregation occurs within the α_2 lamellae, its distribution remains relatively uniform. The limited aggregation neither significantly impedes the coordinated deformation of stacking faults nor leads to the formation of large-scale disordered clusters. The TEM image of the tensile sample at 1200 °C (Figure 3(b)) reveals pronounced lamellar degradation, leading to a sharp decrease in strength. This process induces compositional fluctuations and vacancy aggregation, thereby forming a metastable transition zone [33]. The zone manifests as disordered atomic clusters in simulations. The shear strain contour map in Figure 3(c) indicates higher strain concentrations at disordered atomic regions, leading to the continuous decline in the flow stress.

At 1300 °C, a marked reduction in flow stress was observed in our simulation, a consequence of surpassing the phase transition temperature of TiAl (~1280°C) into the α single-phase region [34]. Meanwhile, the coupling of stress activation and thermal activation makes the deformation mechanism here even more complex. This synergy facilitates intense localized shear, resulting in the nucleation of shear bands characterized by atomic disordering. Figure 3(d) shows at 1300 °C, extensive disordered clusters emerge within α_2 phase and progressively expand into the γ lamella with the strain increased, forming a shear band that runs through both the α_2 and γ phases. The TEM image of deformation microstructure at 1300 °C are shown in Figure 3(e). An obvious shear zone can be observed, which is in good agreement with the simulation results. The diffraction pattern analysis from both sides of the structure demonstrated consistent crystallographic configurations, ruling out the possibility of a domain boundary. The shear strain distribution map in Figure 3(f) reveals significantly higher strain within disordered regions, which will directly lead to material failure. Moreover, the dynamic recrystallization observed in the deformation microstructure at 1300 °C is significantly higher than that at 1200 °C, as shown in Figure A4. This phenomenon also contributes significantly to the decrease in flow stress. To elucidate the formation mechanism of disordered clusters at 1300 °C, an energy-based analysis was conducted. The SFE and disordered cluster energy of α_2-TiAl was simulated and compared at various temperatures, as shown in Figure A1. The results demonstrate that the SFE is approximately 50% lower than that the disordered cluster energy at 1100 and 1200 °C. However, the SFE approaches that of disordered clusters as the temperature rises to 1300 °C, and both mechanisms jointly govern the deformation behavior. Consequently, the marked decline in yield strength at 1300 °C is attributed to the disordered clusters induced shear band.

2.2 Energy density-based temperature-dependent strength model

Based on the study of high-temperature tensile behavior and related atomic mechanisms, PST TiAl exhibit different strength responses across different temperature ranges, particularly around the BDT where strength drops abruptly. Remarkably, the results at 1000 °C vary markedly from those at 1100 and

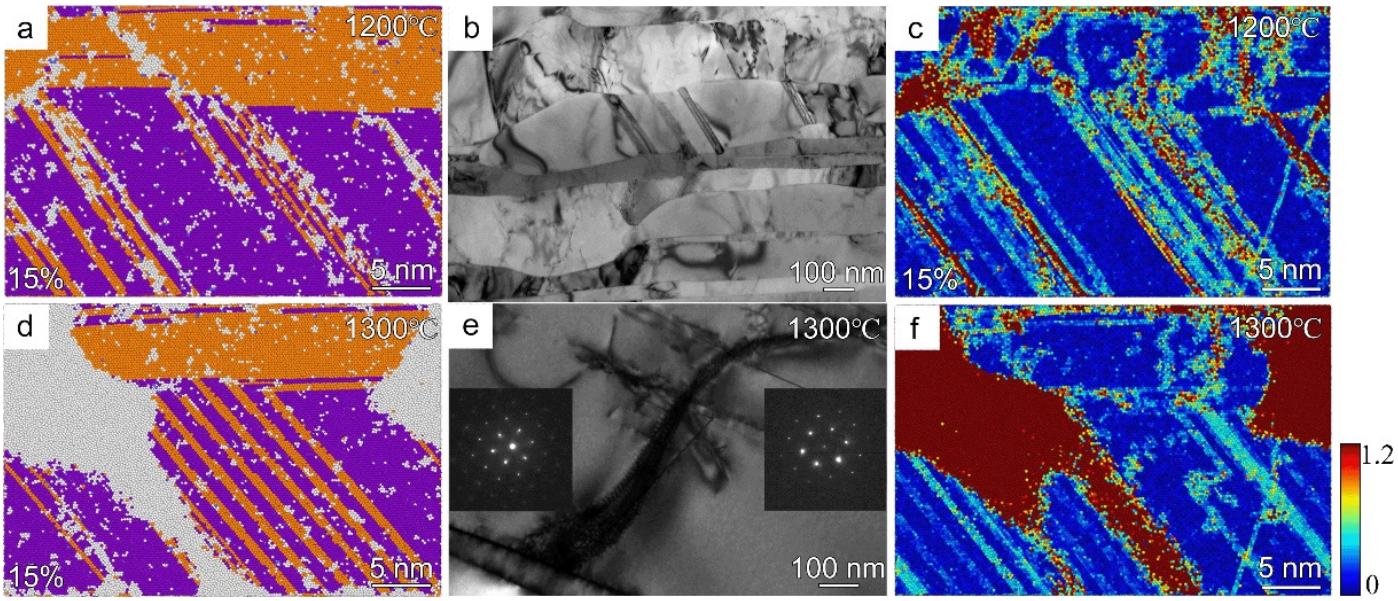


Figure 3. Microstructural characteristics after deformation of PST TiAl through MD simulation, TEM characterization and shear strain contour maps at: (a)–(c) 1200 °C and (d)–(f) 1300 °C.

1200 °C. This divergence is attributed to lamellar degradation by reduces the intrinsic activation energy of α_2-γ phase transformation at higher temperatures, thereby decreasing the high-temperature strength. This abrupt drop in strength leads difficulties for the establishment of the high-temperature strength prediction model. Li et al. [35] proposed a hypothesis that metallic materials yield under a constant critical energy, and they established a temperature-dependent yield strength model based on this assumption. The model suggests that the constant energy primarily consists of two components: one is the thermal energy per unit volume at the yield point, and the other is the elastic deformation energy under the same conditions. The model can effectively describe the stress component evolution (non-thermal stress effect) and the decrease of the intrinsic activation energy through thermal activation (thermal stress effect) nearby the BDT temperature of PST TiAl alloy. Since thermal energy and deformation energy are not entirely equivalent, a conversion coefficient K is introduced to relate the two parameters:

$$W_{\text{total}} = W_d(T) + KW_T(T) \tag{1}$$

where W_{total} is the constant critical energy per unit volume required for crystal yielding. W_d and W_T represent the elastic deformation energy and the thermal energy per unit volume at the yield point (T), with K (assumed constant) is the conversion coefficient between them.

Our analysis identifies disordered atomic cluster as the precursors to both lamellar degradation and shear deformation. The disordered clusters consume a portion of the total energy at high temperatures. Specifically, a portion of the stored constant energy per unit volume is consumed by the crystal to form these disordered clusters, which would otherwise contribute to yielding. Therefore, when calculating the total energy, disordered cluster energy needs to be subtracted. Consequently, we propose a new temperature-dependent yield strength model incorporating thermal energy, deformation energy, and disordered cluster formation energy $W_a(T)$. Based on the assumptions, the critical yield energy is expressed as:

$$W_{\text{total}} = W_d(T) + KW_T(T) - W_a(T) \tag{2}$$

In uniaxial tension, the deformation energy per unit volume can be expressed as:

$$W_d(T) = \frac{(1+\nu_T)}{3E_T}\sigma_y^2(T) \tag{3}$$

The unit volume of thermal energy at temperature T can be expressed as:

$$W_T(T) = \int_0^T \rho Cp(T)dT \tag{4}$$

where $\sigma_y(T)$, ν_T and E_T are the yield strength, Poisson's ratio and Young's modulus respectively at temperature T. $Cp(T)$ is the specific heat capacity

for constant pressure and temperature T, ρ is the density. Here, the cluster energy is represented by subtracting the potential energy at a given temperature from the amorphous energy at a temperature close to the melting point. The results of disordered cluster formation energy is shown in Figure A5. The formula for $W_a(T)$ changes with temperature is fitted and as follows:

$$W_a(T) = 1251 - 0.449 \times T - 1.4 \times 10^{-5} \times T^2 + 8 \times 10^{-8} \times T^3 - 6.54773 \times 10^{-11} \times T^4 \quad (5)$$

When $T = T_m$, there is no effect of deformation energy and disordered cluster energy:

$$W_d(T_m) = 0, \quad W_a(T_m) = 0 \quad (6)$$

where T_m is melting point. Substituting formula (6) into (2) to obtain:

$$W_{\text{total}} = K \int_0^{T_m} \rho Cp(T) dT \quad (7)$$

Substituting $T = T_0$ into equation (2):

$$W_{\text{total}} = \frac{(1+\nu_{T_0})}{3E_{T_0}} \sigma_y^2(T_0) + K \int_0^{T_0} \rho Cp(T) dT - W_a(T_0) \quad (8)$$

Combining equations (7) and (8), we can obtain:

$$K = \frac{(1+\nu_{T_0})\sigma_y^2(T_0) - W_a(T_0)}{3E_{T_0} \int_{T_0}^{T_m} \rho Cp(T) dT} \quad (9)$$

Substituting formula (9) into (2):

$$W_{\text{total}} = \frac{(1+\nu_T)}{3E_T} \sigma_y^2(T) + \frac{(1+\nu_{T_0})\sigma_y^2(T_0) - W_a(T_0)}{3E_{T_0} \int_{T_0}^{T_m} \rho Cp(T) dT} \int_0^T \rho Cp(T) dT - W_a(T) \quad (10)$$

Combining formulas (10) and (7):

$$\sigma_y(T) = \left[\frac{3E_T}{(1+\nu_T)} \left(\frac{1+\nu_{T_0} - 3E_{T_0} W_a(T_0)}{3E_{T_0} \int_{T_0}^{T_m} \rho Cp(T) dT} \left[\int_T^{T_m} \rho Cp(T) dT + W_a(T) \right) \right] \right]^{\frac{1}{2}} \quad (11)$$

Figure 4 presents a comparison of the yield stress of PST TiAl from the model predictions based on equation (11) and our MD simulation results. The BDT behaviour seen in the simulations below a critical temperature is well captured by the model. Below the BDTT, curve from equation (1) indicates before strength softening occurs in PST TiAl, provided that the energy density equation remains valid before 900 °C. As shown in Figure 4, both simulations and the theory consistently display that disordered atomic clusters as the precursors to lamellar degradation governs the BDT behavior of PST TiAl. We predict the BDTT is over 1000 °C in PST TiAl.

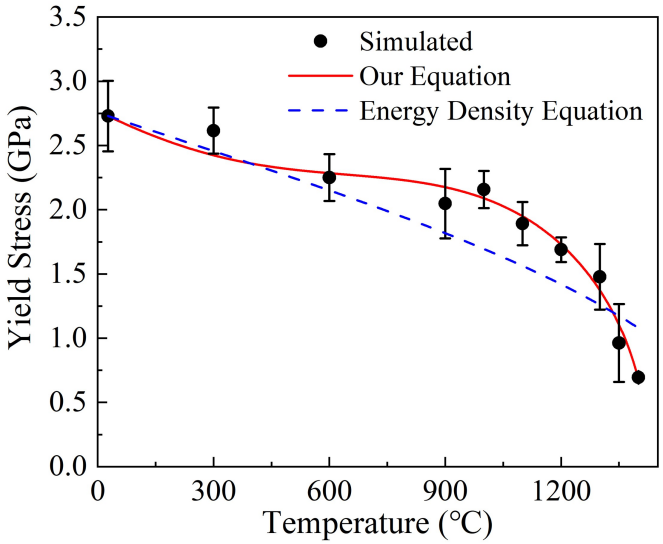


Figure 4. Yield stress of PST TiAl as a function of temperature. MD simulation for yield stress are shown together with our equation and typical energy density equation.

3 Conclusions

Our study reveals a novel mechanism for the BDT in PST TiAl, which deviates significantly from conventional views in other intermetallic compounds. It is established that the BDT is primarily driven by lamellar degradation, rather than by thermally activated dislocation actions or dynamic recrystallization. Our findings demonstrate that this lamellar degradation is a direct consequence of the $\alpha_2 \rightarrow \gamma$ phase transformation occurring at the critical BDT temperature, originating from an anomalous increase in the stacking fault energy of the α_2 phase. Furthermore, the unconventional transition is effectively described by our established energy density-based strength model. This study provides fundamental new insights into the high-temperature deformation behavior of intermetallic compounds and opens new avenues for designing advanced intermetallic compounds for elevated-temperature applications.

4 Simulation and experimental section

4.1 Experimental and material testing

The experimental subjects of this study, PST TiAl, are highly consistent with the simulated conditions. The details of the composition and microstructure have been mentioned in the previously published reports. Tensile tests were performed utilizing an Instron 5969 electromechanical universal testing machine equipped with an integrated environmental chamber for heating. Specimens were cylindrical rods with a length of 76 mm, tested at a strain rate of 10^{-3} s^{-1}. Deformation microstructures were characterized via a cold field-emission transmission electron microscope (JEOL, JEM-F200) along the $< 011]$ zone axis. The TEM samples were extracted after stretching and ground to a thickness of 70 μm using progressively finer sandpapers. Subsequently, electron-transparent regions were prepared using a Twin-Jet Electropolisher, with the electrolyte solution composed of perchloric acid, methanol, and n-butanol in a volumetric ratio of 1:5:10.

4.2 Simulation methods

In this work, MD simulations were conducted to investigate interatomic mechanisms of TiAl system using the large-scale atomic/molecular massively parallel simulator (LAMMPS). Atomic interactions were described using the embedded atom method (EAM) potential [36]. The model of PST TiAl developed in this study consists of γ-TiAl and α_2-Ti_3Al phases. The unique lamellar structure was visualized using the post-processing software OVITO [37], as shown in Figure A6(a). The entire model has dimensions of approximately $17.86 \times 33.47 \times 68.21$ nm^3 and contains $2,509,498$ atoms. The structure is divided into four lamellae: the top lamella is the α_2-Ti_3Al phase with a thickness of approximately 9.71 nm, while the bottom three layers consist of the γ phase with a total thickness of approximately 19.50 nm. The γ-TiAl and α_2-Ti_3Al phases follow the Blackburn orientation relationship: $(111)_\gamma // (0001)_{\alpha_2}$ and $< 1\bar{1}0 >_\gamma // < 1\bar{2}10 >_{\alpha_2}$. The interface between the two phases is illustrated in Figure A6(b, e). Additionally, $< 1\bar{1}0 >_\gamma // < 1\bar{2}10 >_{\alpha_2}$, $< \bar{1}\bar{1}2 >_\gamma // < \bar{1}010 >_{\alpha_2}$, $< 111 >_\gamma // < 0001 >_{\alpha_2}$ in both phases are aligned parallel to the x-, y-, and z-axis, respectively. Two distinct interfaces were constructed between the three γ-phase layers based on the actual material structure. The interfaces in the model from top to bottom are as follows: the phase interface between γ_1 and α_2, the pseudo-twin interface between γ_1 and γ_2, and the true twin interface between γ_2 and γ_3 (Figure A6(b-d). In the true twin interface (Figure A6(g)), the $\{111\}$ planes of two adjacent γ_2 and γ_3 lamella rotated $180°$ around the $< 111]$ direction to keep $< 1\bar{1}0]$ and $< 11\bar{2}]$ directions of the matrix parallel to the $< \bar{1}10]$ and $< \bar{1}\bar{1}2]$ directions of the twin. However, the $\{111\}$ planes of two γ lamellae rotates around $< 111]$ by $60°$ in the pseudo twin interface (Figure A6(f)). The polycrystal TiAl alloy structure was constructed by an open-source software Atomsk. As shown in Figure A7, the simulation box is $20 \times 30 \times 20$ nm^3, which contains 736182 atoms. It was composed of 12 grains with random orientation.

During the simulation process, periodic boundary conditions are adopted. At first, perform energy minimization on the system, the system was relaxed by conjugate gradient method [38]. Subsequently, the system was equilibrated by applying isothermal-isobaric ensemble (NPT) to enable the relaxation residual domain stress. The NPT ensemble ensures that the number of atoms, pressure, and temperature of the simulated system remain constant during the tensile process. In the simulation, the system was subjected to a uniaxial tensile loading at a strain rate of 1.0×10^8 s^{-1} along the loading direction, and the timestep was set to 0.001 ps. Tensile loading direction was y-axis. While the strain rate in MD is significantly higher than in experiments, the qualitative trends remain comparable as the underlying deformation mechanisms [39]. After the simulation is completed, the material structure can be observed through the visualization post-processing software OVITO. The Atomic Strain and Color Coding was adopted to draw the atomic stress cloud map. The Polyhedral template matching (PTM) [40] was chosen to identify all structural changes and evolution of deformation mechanisms during the deformation process.

Data Availability Statement

Data will be made available on request.

Funding

This work was supported in part by the National Natural Science Foundation of China under Grant 12202201, Grant 52571145, Grant 92463301, Grant 52433016, Grant 92163215, Grant 52305379, and Grant 52174364; in part by the Natural Science Foundation of Jiangsu Province under Grant BK20220918, Grant BK20243066, and Grant BE2023024; in part by

the Fundamental Research Funds for the Central Universities under Grant 30922010711 and Grant 30922010202; in part by the Development Funds of State Key Laboratory of Materials Processing and Die & Mould Technology, Huazhong University of Science and Technology under Grant P2024-004.

Conflicts of Interest

The authors declare no conflicts of interest.

Ethical Approval and Consent to Participate

Not applicable.

References

[1] Tiwari, R., Tewari, S. N., Asthana, R., & Garg, A. (1995). Mechanical properties of extruded dual-phase NiAl alloys. *Journal of materials science, 30*(19), 4861-4870. [Crossref]

[2] Booth, A. S., & Roberts, S. G. (1997). The brittle-ductile transition in γ-TiAl single crystals. *Acta materialia, 45*(3), 1045-1053. [Crossref]

[3] Tanaka, M., Tarleton, E., & Roberts, S. G. (2008). The brittle–ductile transition in single-crystal iron. *Acta Materialia, 56*(18), 5123-5129. [Crossref]

[4] Zhang, Y. H., & Han, W. Z. (2021). Mechanism of brittle-to-ductile transition in tungsten under small-punch testing. *Acta Materialia, 220*, 117332. [Crossref]

[5] Chen, R., Wang, Q., Yang, Y., Guo, J., Su, Y., Ding, H., & Fu, H. (2018). Brittle–ductile transition during creep in nearly and fully lamellar high-Nb TiAl alloys. *Intermetallics, 93*, 47-54. [Crossref]

[6] Zhang, S., Tian, N., Li, D., Li, J., Jin, F., Wang, G., & Tian, S. (2022). Microstructure evolution and fracture mechanism of a TiAl–Nb alloy during high-temperature tensile testing. *Materials Science and Engineering: A, 831*, 142094. [Crossref]

[7] Li, L. L., Su, Y., Beyerlein, I. J., & Han, W. Z. (2020). Achieving room-temperature brittle-to-ductile transition in ultrafine layered Fe-Al alloys. *Science Advances, 6*(39), eabb6658. [Crossref]

[8] Šmida, T., & Magula, V. (2014). Brittle to ductile transition–An engineer's point of view. *Materials & Design (1980-2015), 54*, 582-586. [Crossref]

[9] Schafrik, R. E. (2016). Materials for a non-steady-state world. *Metallurgical and Materials Transactions B, 47*(3), 1505-1515. [Crossref]

[10] Clemens, H., & Mayer, S. (2016). Intermetallic titanium aluminides in aerospace applications–processing, microstructure and properties. *Materials at high temperatures, 33*(4-5), 560-570. [Crossref]

[11] Chen, G., Peng, Y., Zheng, G., Qi, Z., Wang, M., Yu, H., ... & Liu, C. T. (2016). Polysynthetic twinned TiAl single crystals for high-temperature applications. *Nature Materials, 15*(8), 876-881. [Crossref]

[12] Chen, Y., Cao, Y., Qi, Z., & Chen, G. (2021). Increasing high-temperature fatigue resistance of polysynthetic twinned TiAl single crystal by plastic strain delocalization. *Journal of Materials Science & Technology, 93*, 53-59. [Crossref]

[13] Yan, S., Qi, Z., Chen, Y., Cao, Y., Zhang, J., Zheng, G., ... & Chen, G. (2021). Interlamellar boundaries govern cracking. *Acta Materialia, 215*, 117091. [Crossref]

[14] Zheng, G., Chen, Y., Xiang, H., Zhang, J., Tu, K. N., Feng, C., ... & Chen, G. (2023). Coupled nucleation of dual-phase lamellar structure. *The Innovation Materials, 1*(3), 100043. [Crossref]

[15] Imayev, V. M., Imayev, R. M., & Salishchev, G. A. (2000). On two stages of brittle-to-ductile transition in TiAl intermetallic. *Intermetallics, 8*(1), 1-6. [Crossref]

[16] Zhao, W., & Luzzi, D. E. (2000). Characterizations of lamellar interfaces and segregations in a PST-TiAl intermetallic alloy by an analytical scanning transmission electron microscope. *MRS Online Proceedings Library, 652*(1), 104. [Crossref]

[17] Kim, H. Y., & Maruyama, K. (2001). Parallel twinning during creep deformation in soft orientation PST crystal of TiAl alloy. *Acta materialia, 49*(14), 2635-2643. [Crossref]

[18] Meyers, M. A., & Chawla, K. K. (2008). *Mechanical behavior of materials*. Cambridge university press. [Crossref]

[19] Chang, Y. A., & Himmel, L. (1966). Temperature dependence of the elastic constants of Cu, Ag, and Au above room temperature. *Journal of Applied Physics, 37*(9), 3567-3572. [Crossref]

[20] Brotzu, A., Felli, F., Marra, F., Pilone, D., & Pulci, G. (2018). Mechanical properties of a TiAl-based alloy at room and high temperatures. *Materials Science and Technology, 34*(15), 1847-1853. [Crossref]

[21] Appel, F., Paul, J. D. H., & Oehring, M. (2011). *Gamma titanium aluminide alloys: science and technology*. John Wiley & Sons. [Crossref]

[22] Wang, Q., Chen, R., Chen, D., Su, Y., Ding, H., Guo, J., & Fu, H. (2019). The characteristics and mechanisms of creep brittle-ductile transition in TiAl alloys. *Materials Science and Engineering: A, 767*, 138393. [Crossref]

[23] Zhang, M., Yang, S., & Wan, F. (2019). Competition mechanism of brittle–ductile transition of metals under tensile condition. *Mechanics of Materials, 137*, 103138. [Crossref]

[24] Paidar, V., Pope, D. P., & Vitek, V. (1984). A theory of the anomalous yield behavior in L12 ordered alloys. *Acta Metallurgica, 32*(3), 435-448. [Crossref]

[25] Hirsch, P. B. (1992). A model of the anomalous yield stress for (111) slip in L12 alloys. *Progress in materials science, 36*, 63-88. [Crossref]

[26] Zhu, Y., Yi, M., Zhang, Z., & Guo, W. (2025). Role of true and pseudo twin boundary in high-temperature creep of γ-TiAl alloy: Atomistic mechanism and mesoscale model. *Acta Materialia*, 121418. [Crossref]

[27] Wu, Z. X., Zhang, Y. W., & Srolovitz, D. J. (2009). Dislocation–twin interaction mechanisms for ultrahigh strength and ductility in nanotwinned metals. *Acta Materialia, 57*(15), 4508-4518. [Crossref]

[28] Qiu, L., Wang, S., Zhou, X., Lu, Z., Huang, X., Feng, X., ... & Chen, G. (2025). Phase Transformation Induced Plastic Deformation Mechanism in α2-Ti3Al. *Interdisciplinary Materials, 4*(3), 524-534. [Crossref]

[29] Zghal, S., Thomas, M., Naka, S., Finel, A., & Couret, A. (2005). Phase transformations in TiAl based alloys. *Acta materialia, 53*(9), 2653-2664. [Crossref]

[30] Denquin, A., & Naka, S. (1996). Phase transformation mechanisms involved in two-phase TiAl-based alloys—I. Lambellar structure formation. *Acta materialia, 44*(1), 343-352. [Crossref]

[31] Feng, L., Kannan, S. B., Egan, A., Smith, T., Mills, M. J., Ghazisaeidi, M., & Wang, Y. (2022). Localized phase transformation at stacking faults and mechanism-based alloy design. *Acta Materialia, 240*, 118287. [Crossref]

[32] Chen, G. L., Zhang, L. C., & Zhang, W. J. (1999). Microstructural stability of lamellar TiAl-based alloys at high temperature. *Intermetallics, 7*(11), 1211-1218. [Crossref]

[33] Liu, Y., Li, J., Tang, B., Song, L., Wang, W. Y., Liu, D., ... & Kou, H. (2023). Decomposition and phase transformation mechanisms of α2 lamellae in β-solidified γ-TiAl alloys. *Acta Materialia, 242*, 118492. [Crossref]

[34] Chen, G. L., Zhang, W. J., Liu, Z. C., Li, S. J., & Kim, Y. W. (1999). Microstructure and properties of high-Nb containing TiAl-base alloys. *Gamma titanium aluminides, 1999*.

[35] Li, W., Zhang, X., Kou, H., Wang, R., & Fang, D. (2016). Theoretical prediction of temperature dependent yield strength for metallic materials. *International Journal of Mechanical Sciences, 105*, 273-278. [Crossref]

[36] Zope, R. R., & Mishin, Y. (2003). Interatomic potentials for atomistic simulations of the Ti-Al system. *Physical Review B, 68*(2), 024102. [Crossref]

[37] Stukowski, A. (2009). Visualization and analysis of atomistic simulation data with OVITO–the Open Visualization Tool. *Modelling and simulation in materials science and engineering, 18*(1), 015012. [Crossref]

[38] Štich, I., Car, R., Parrinello, M., & Baroni, S. (1989). Conjugate gradient minimization of the energy functional: A new method for electronic structure calculation. *Physical Review B, 39*(8), 4997. [Crossref]

[39] Li, X., Wei, Y., Lu, L., Lu, K., & Gao, H. (2010). Dislocation nucleation governed softening and maximum strength in nano-twinned metals. *Nature, 464*(7290), 877-880. [Crossref]

[40] Larsen, P. M., Schmidt, S., & Schiøtz, J. (2016). Robust structural identification via polyhedral template matching. *Modelling and Simulation in Materials Science and Engineering, 24*(5), 055007. [Crossref]

Appendix

Content:

1. Figure A1: Comparison of stacking fault energy and disordered cluster formation energy.
2. Figure A2: Shear strain map of PST TiAl.
3. Figure A3: Microstructure characteristics and shear strain distribution of polycrystal TiAl.
4. Figure A4: Microstructural characteristics of PST TiAl through TEM characterization after deformation at 1200 ℃ and 1300 ℃ .
5. Figure A5: Fitting results of disordered cluster formation energy.
6. Figure A6: Schematic diagram of modeling structure and interface.
7. Figure A7: Polycrystal γ-TiAl tensile model.

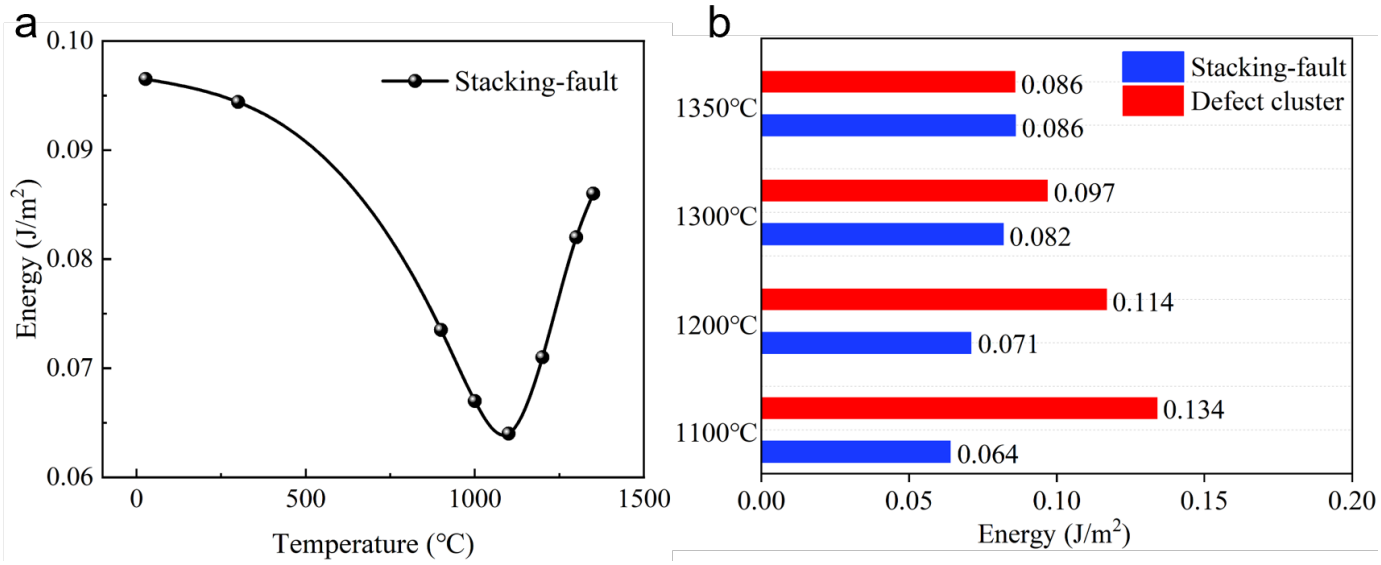


Figure A1. (a) The stacking fault energy at different temperatures of α_2 phase. (b) Comparison of stacking fault energy and disordered cluster formation energy at 1100 1350 °C of α_2 phase.

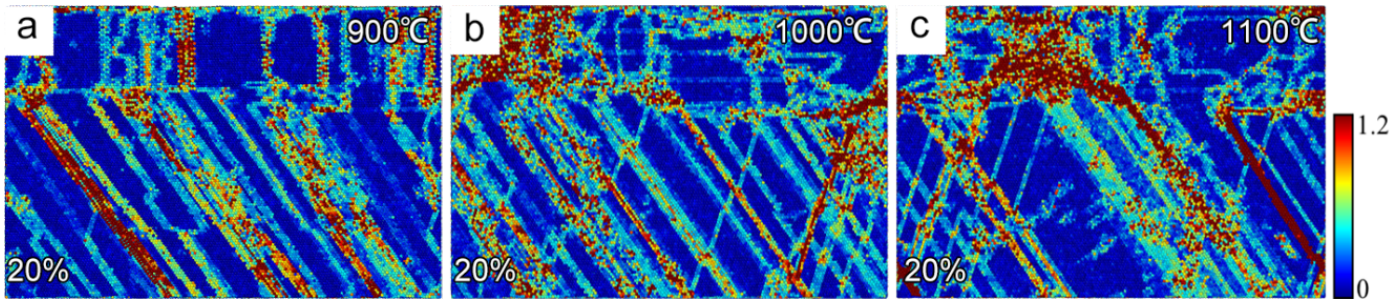


Figure A2. Shear strain map of PST TiAl at 20% strain under: (a) 900 °C, (b) 1000 °C, (c) 1100 °C.

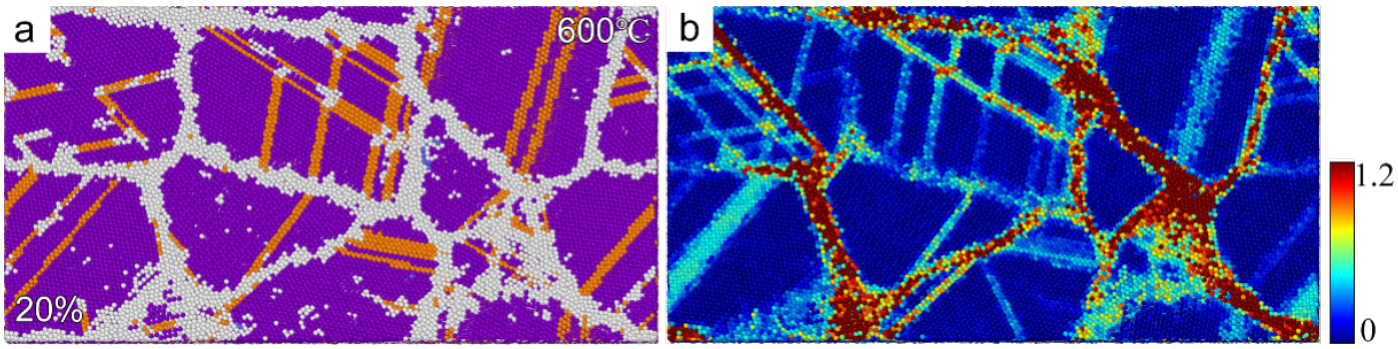


Figure A3. (a) Microstructural characteristic and (b) shear strain of polycrystal TiAl at strain 20% and temperature 600 °C.

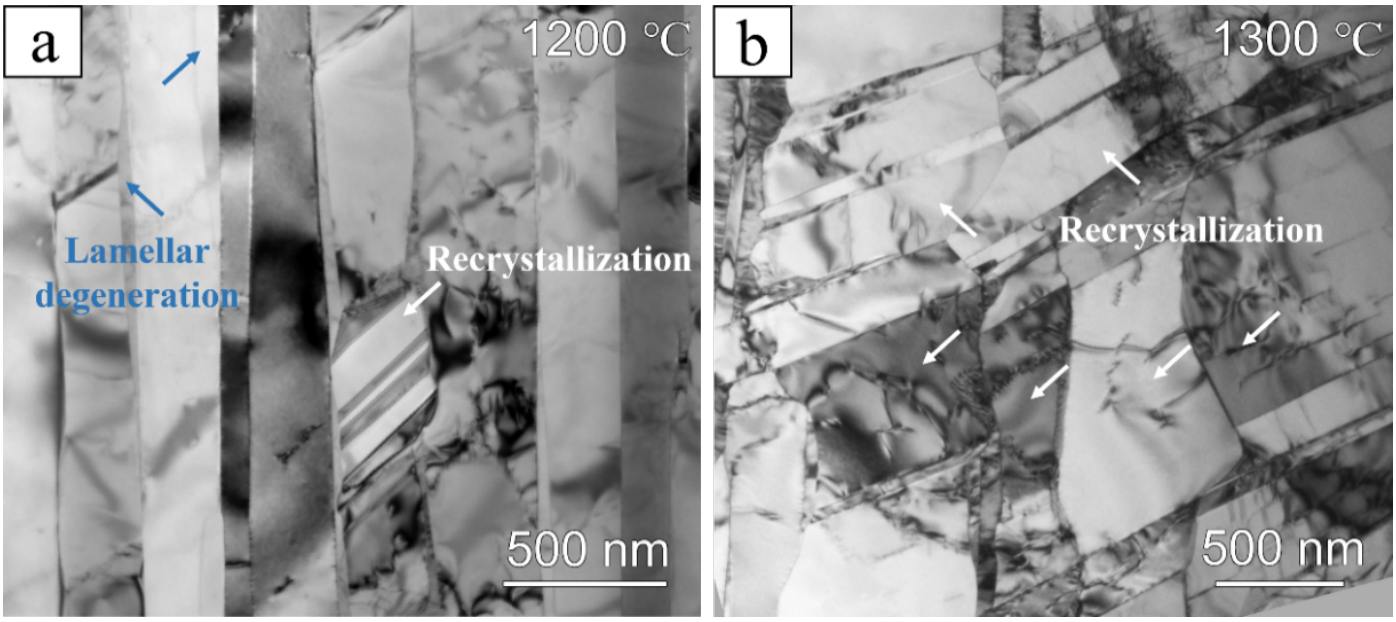


Figure A4. Microstructural characteristics of PST TiAl through TEM characterization after deformation at: (a) 1200 °C and (b) 1300 °C.

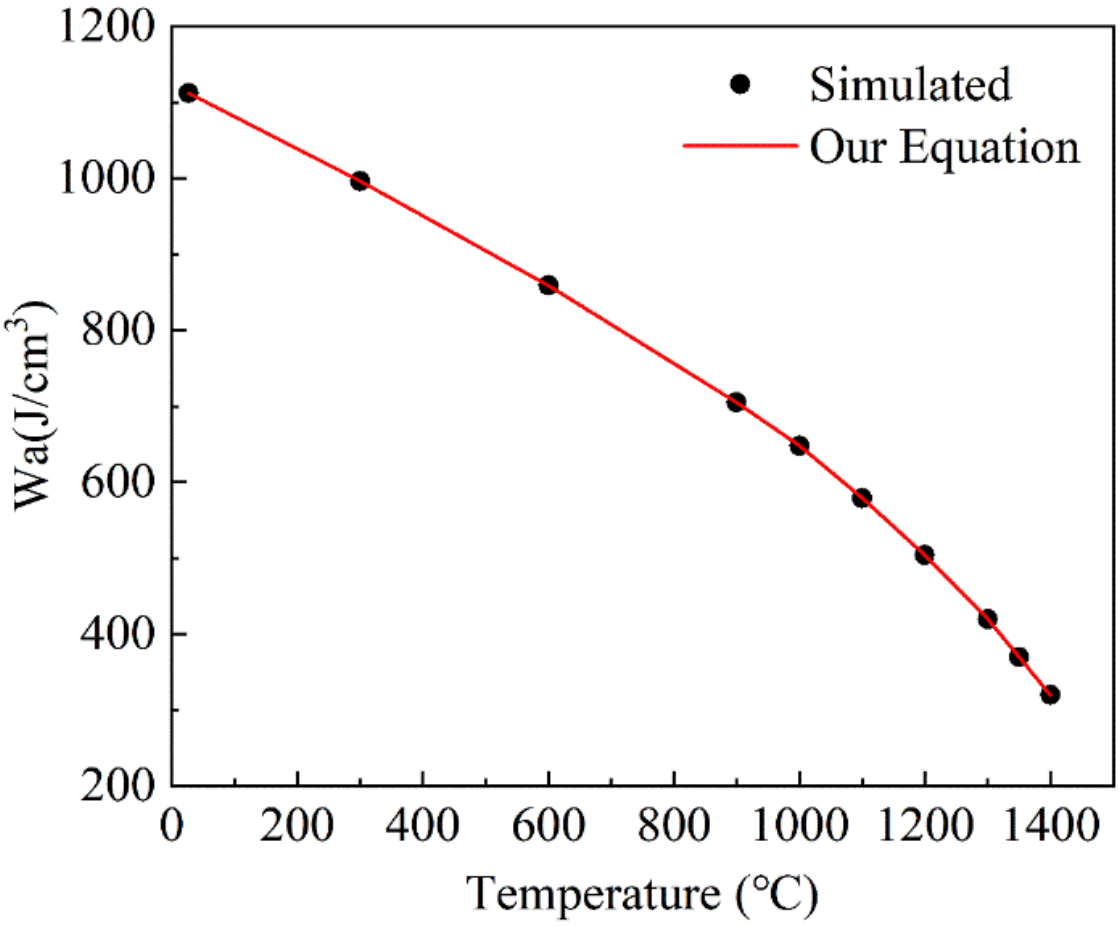


Figure A5. Fitting results of disordered cluster formation energy formula.

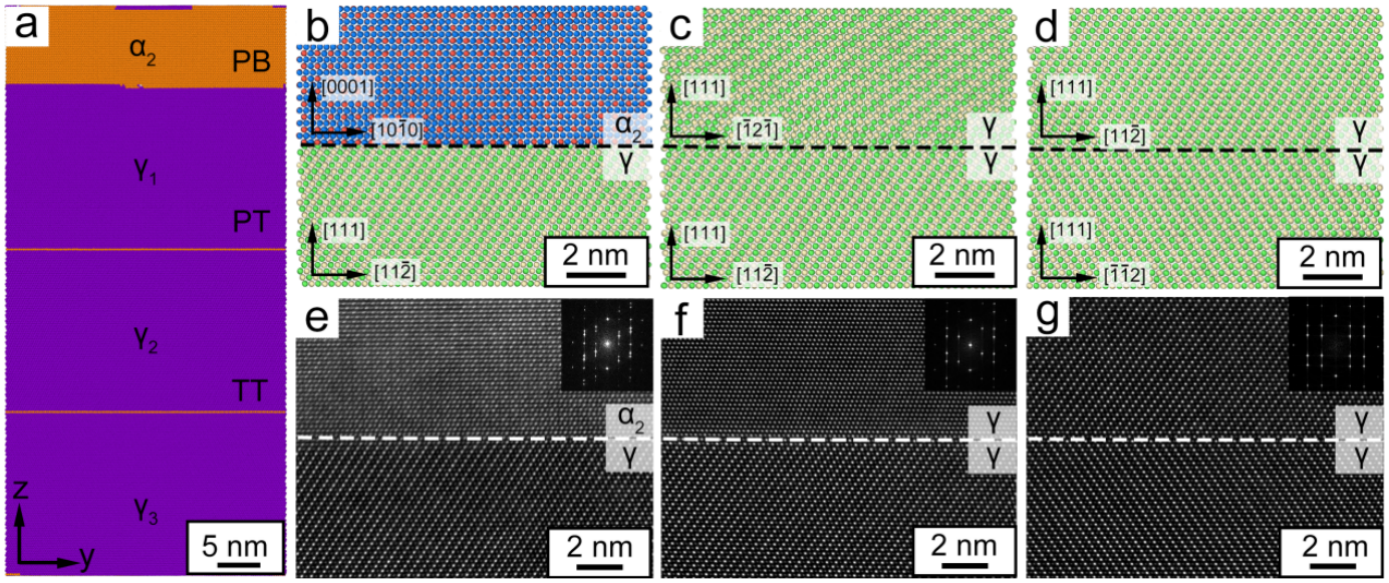


Figure A6. Schematic diagrams of modeling structure and interfaces: (a) PST TiAl tensile model, (b), (e) $\gamma 2/\gamma 1$ phase boundary, (c), (f) Pseudo twin grain boundary, (d), (g) True twin grain boundary.

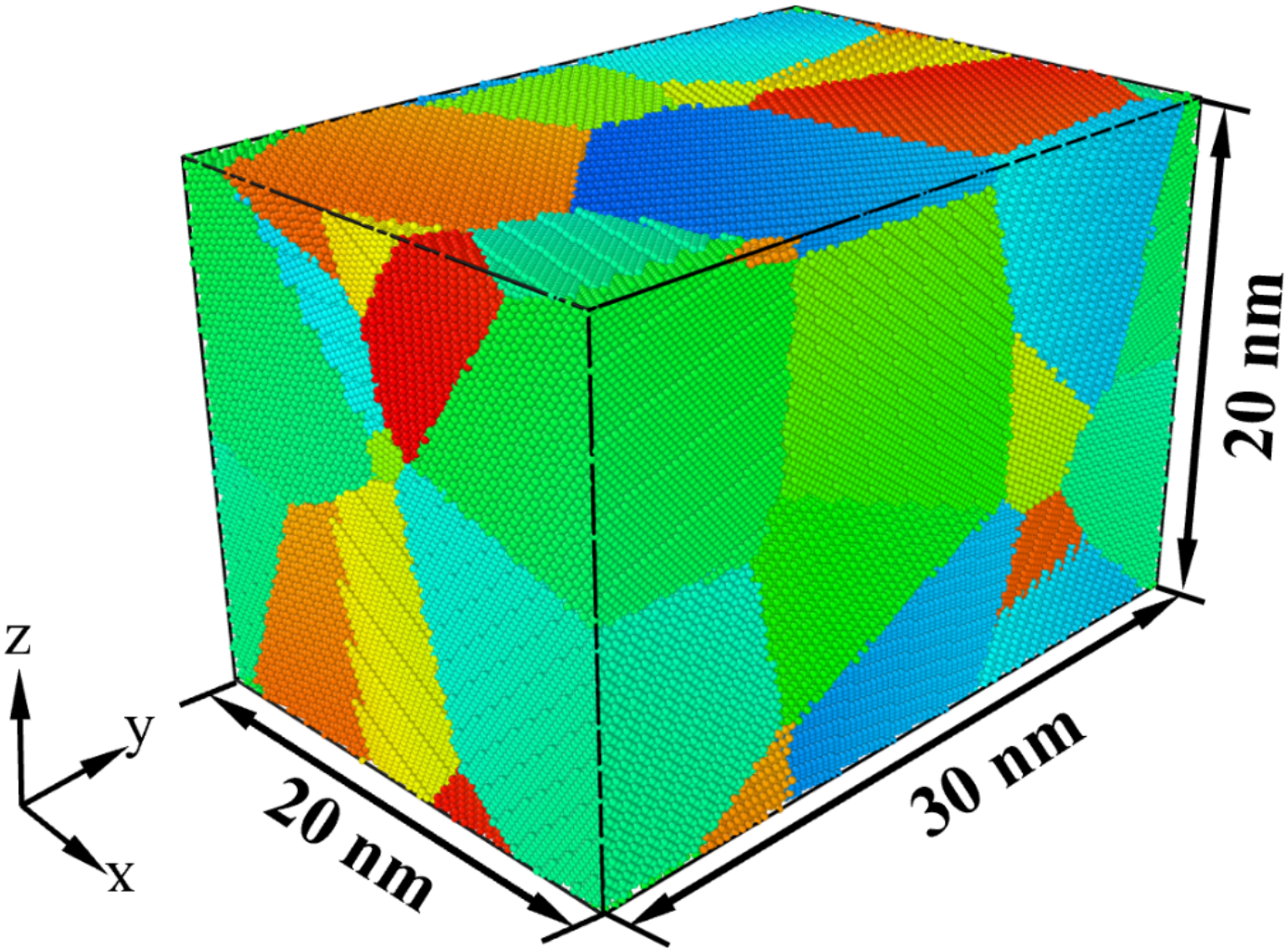


Figure A7. Tensile model of polycrystal γ-TiAl.



Henggao Xiang is a professor at Nanjing University of Science and Technology in China. He earned his BS degree from Nanjing Agricultural University, his MS degree from Chongqing University, and his PhD degree from Nanjing University of Aeronautics and Astronautics. His research interest focuses on lightweight material behavior and evaluation. (Email: hqxiang@njust.edu.cn)



Demin Zhu is a PhD student at Nanjing University of Science and Technology, China. His research focuses on pre-deformation and recovery mechanisms of heat treatment in TiAl alloys. (Email: zhudemin@njust.edu.cn)



Xu Liu is a PhD student at Nanjing University of Science and Technology, China. His research focuses on theoretical calculation and strengthening mechanisms of TiAl alloys. (Email: wxliuxu@njust.edu.cn)



Yang Chen is a professor at Nanjing University of Science and Technology, China. He earned his BS degree from the Georgia Institute of Technology and his MS degree from the University of Michigan, Ann Arbor. After obtaining his PhD degree in materials science and engineering from the University of California, Los Angeles, he became a research scientist at Nanjing University of Science and Technology in 2020. His research is mainly focused on advanced manufacturing and characterization of metallic and intermetallic materials. (Email: yang.chen@njust.edu.cn)



Zhixiang Qi is a professor at Nanjing University of Science and Technology, China. He received his BS degree in 2014 and his PhD degree in 2019 from the School of Materials Science and Engineering, Nanjing University of Science and Technology, under the guidance of Prof. Guang Chen. He is currently the director of the Jiangsu Engine Materials Engineering Research Center. His research interest focuses on the directional solidification and intermetallic compound material technology. (Email: zxqi@njust.edu.cn)



Guang Chen is a distinguished professor at Nanjing University of Science and Technology, China. He is the member of the Chinese Academy of Sciences, a National Teaching Master, a recipient of the National May 1st Labor Medal and the inaugural National Award for Excellence in Innovation. His research interests include fundamental research and engineering applications of lightweight heat-resistant intermetallics, directional solidification of superalloys, amorphous composites, and steel processing. (Email: gchen@njust.edu.cn)